Available online at www.sciencedirect.com
ScienceDirect
Trans. Nonferrous Met. Soc. China 20(2010) 1702−1706
Transactions of Nonferrous Metals Society of China
www.tnmsc.cn

Evaluation of pitting corrosion of thixoformed A356 alloy using a simulation model

S. TAHAMTAN, A. FADAVI BOOSTANI

Department of Materials Engineering, Isfahan University of Technology (IUT), Isfahan, Iran

Received 13 May 2010; accepted 25 June 2010

Abstract: Pitting behavior of thixoformed A356 alloy, with different reheating temperatures, was evaluated. Linear sweep voltammetric tests were used to study the pitting behavior of thixoformed, rheocast and gravity-cast A356 alloy in a 3.5% NaCl solution. A simulation method was also used in order to identify local galvanic corrosion current density between local galvanic couples. The results obtained show that the resistance to pitting corrosion of the thixoformed samples formed at 600 °C is higher than that of the samples formed at 610 °C as well as rheocast and gravity-cast samples. These results could be explained by morphological aspects of silicon phase as well as the area effect as related to galvanic corrosion between silicon particles and eutectic aluminum phase.

Key words: rheocasting; gravity casting; A356 alloy; corrosion; pitting; pitting; microstructure

1 Introduction

After more than 30 years development, the semi-solid metal process has now been accepted as an excellent net shape metal forming method[1]. Semi-solid metals and processing techniques are entering into the commercialisation stage for various industrial applications, including automobile and electronic industries, owing to the extensive research efforts in the last 10 years[1−5].

Semi-solid A356 and A357 alloys are susceptible to pitting corrosion in chloride media[5−7]. Pitting is the most common form of aluminum corrosion, particularly in solutions containing halide ions, of which Cl^- is the most frequently encountered[8−12]. The presence of chloride ions causes the localized breakdown of the passive film, which leads to initiation and growth of corrosion pits[13]. The resistance of aluminum to pitting depends significantly on its purity[8, 14]. This is because localized corrosion such as pitting is caused by a difference in corrosion potential in a local cell formed in or on the metal surface by the presence of anodic or cathodic microconstituents such as insoluble intermetallic compounds or single elements, such as $CuAl_2$, $FeAl_3$ and silicon[8].

Corrosion properties of semi-solid alloys were largely unexplored. Corrosion properties of thixoformed A357 alloy with different reheating temperatures as well as corrosion properties of permanent mold cast A357 alloy have been studied during the last 5 years[5−6]. It has been reported that corrosion properties of A357 and A356 alloys were greatly improved by thixoforming process compared with permanent mold and rheocast processes[5−6]. PARK et al[2] and YU et al[5] related the improvement of corrosion properties to microstructural changes by thixoforming process qualitatively.

The purpose of this work is to study the effect of microstructural features on pitting behavior of thixoformed A356 alloy, with different reheating temperatures, quantatively. The results are then compared with those of rheocast and gravity-cast A356 alloy.

2 Experimental

In this study, A356 alloy was produced by melting high purity aluminum and mixing with high purity silicon and magnesium. Table 1 shows the chemical composition of the alloy used in this study. All the samples were rheocast using a mechanical stirrer type rheocaster machine. For this purpose, A356 alloy was heated to 50 °C above its liquidus temperature(623 °C)

Corresponding author: S. TAHAMTAN; Tel: +98-9177108449; E-mail: salehtahamtan59@yahoo.com
DOI: 10.1016/S1003-6326(09)60361-7

and then cooled down to 620 °C, where mechanical stirring at 1 000 r/min was started. Mechanical stirring was continued within the temperature range of 620−578 °C. When the semi-solid mixture reached to 578 °C, corresponding to 60% solid fraction, the slurry was bottom-poured into a metallic mold. In order to homogenize the composition, the ingots were reheated to 435 °C, held for 5 h and then quenched into water[5]. The specimens were consequently reheated to 600 °C or 610 °C in an electric muffle furnace with ±2 °C temperature accuracy and held at these temperatures for 10 min.

Table 1 Chemical composition of A356 alloy used in this study (mass fraction, %)

Si	Fe	Cu	Mn	Mg	Ti	Zn	Al
6.97	0.15	<0.05	<0.02	0.3	0.01	0.04	Bal.

Temperature of the specimens was measured using a calibrated K-type thermocouple located near the centre of the top surface of the specimens. The holding time was measured from the moment that the furnace reached the required temperature. The holder with the die and specimens were then transferred from the furnace to the platform on the press and 50% hot working was applied. In order to prevent the specimens from cooling during hot working, the forming die and the holder were all heated to the same temperatures as the specimens in the furnace.

In order to study the pitting behavior, linear sweep voltammetric (LSV) tests were performed on the thixoformed, rheocast and gravity-cast A356 samples in a 3.5% NaCl solution at a scanning rate of 1 mV/s. Measurement of galvanic corrosion current versus time as well as LSV test was performed using an EG&G model 273A potentiostat.

The following parameters were determined for each sample using image analysis techniques:

1) Area equivalent diameter (D): equivalent diameter of a particle whose area is equal to the average area of silicon particle.

2) Anode area to cathode area ratio (A_c/A_a) was calculated using Eq.(1):

$$A_c / A_a = A/(P \cdot W) \quad (1)$$

where A is the silicon area, P is the silicon perimeter and W is the mean width of corroded zone around silicon particle. The mean width of corroded zone around silicon particles was calculated using high magnification microscopy. Calculations of area equivalent diameter and anode area to cathode area ratio of all samples were performed on at least 5 images. The surface of all tested specimens was examined using a Nikon optical microscope (OM) model Epiphoto300 and a Philips-XH3 scanning electron microscope (SEM).

3 Results and discussion

Fig.1 shows the optical microstructures of A356 samples produced by gravity-casting (Fig.1(a)) and rheocasting (Fig.1(b)) processes. In the case of gravity-cast samples, typical dendritic shape of primary α phase is observed, whereas in the case of rheocast samples, equiaxed primary α phase is found to be distributed throughout the matrix. Fig.2 shows the optical microstructures of thixoformed samples at the reheating temperatures of 600 °C (Fig.2(a)) and 610 °C (Fig.2(b)). Optical microstructures of the eutectic zone in the above specimens are also documented. Figs.1 and 2 demonstrate a substantial microstructural difference in the shape and size of eutectic silicon particles.

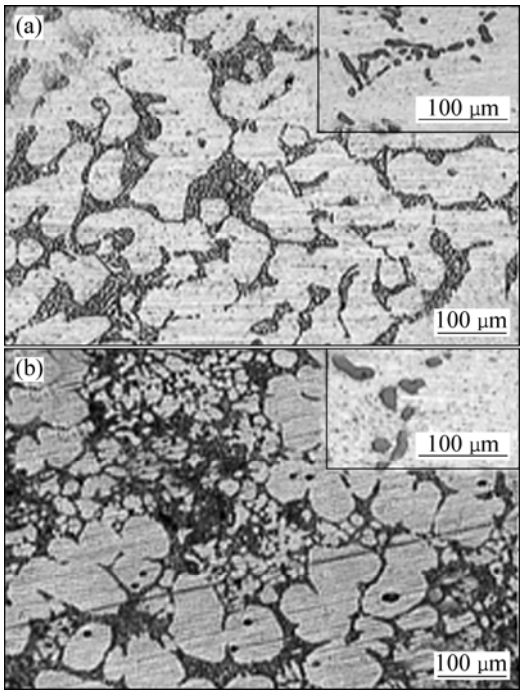

Fig.1 Optical microstructures of A356 samples produced using different processing routes: (a) Gravity-cast; (b) Rheocast

Quantitative metallographic evaluation of the various microstructural features and defects was carried out to compare the various cast microstructures produced. These results are shown in Table 2. Compared with gravity-cast and rheocast processes, thixoforming process decreases area equivalent diameter of silicon particles and porosity.

Table 3 shows the results of LSV test on the thixoformed, rheocast and gravity-cast A356 samples. It is clearly demonstrated that thixoforming process is extremely beneficial for improving corrosion resistance of A356 samples compared with that of rheocast and gravity-cast samples. In the case of thixoformed samples,

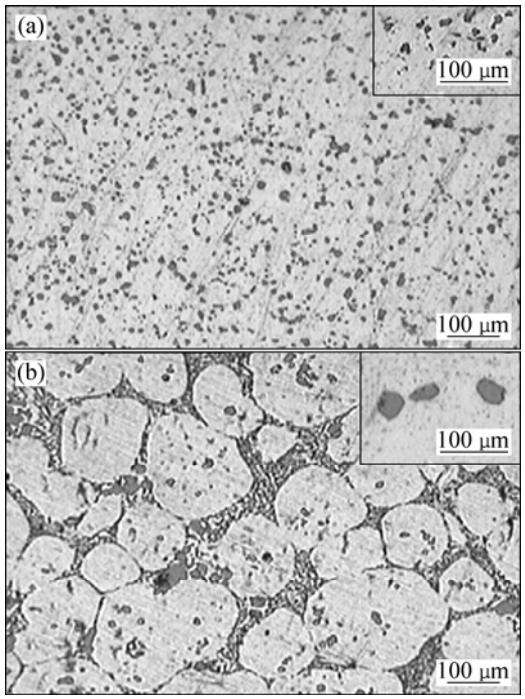

Fig.2 Optical microstructures of thixoformed A356 samples 50% hot-worked at different temperatures: (a) 600 °C; (b) 610 °C

Table 2 Results of quantitative metallographic evaluation for microstructures under investigation

Sample	Area equivalent diameter of Si particles/μm	Porosity volume fraction/%
Gravity-cast	11.4±0.21	13.21±1.4
Rheocast	7.99±0.23	3.00±0.3
Thixoformed at 600 °C	3.99±0.21	0.24±0.11
Thixoformed at 610 °C	4.11±0.15	0.41±0.14

Table 3 LSV test results of thixoformed, rheocast and gravity-cast A356 samples after exposure in 3.5% NaCl solution

Sample	Pitting potential (vs SCE)/mV	Passive film stability range (vs SCE)/mV
Gravity-cast	−848±11.01	71.1±9.11
Rheocast	−690±8.21	77±6.12
Thixoformed at 600 °C	−599±3.99	300±5.74
Thixoformed at 610 °C	−610±6.11	205±7.32

passive film stability range (PFSR) and φ_P are increased, implying the impediment to pit initiation.

Fig.3 shows the SEM image of corroded sample after LSV test in a 3.5% NaCl solution (thixoformed sample formed at 610 °C). As it is seen, the pitting corrosion occurs selectively in the eutectic area, while primary α phase (the composition of which is almost 100% pure aluminum) is mostly protected, regardless of processing route. In the eutectic area, corrosion mostly occurs around the silicon particles. So, silicon particles act as local cathodes with respect to the eutectic aluminum phase and contribute to localized corrosion of surrounding matrix areas. When galvanic coupling is the main cause of corrosion, the area ratio of noble to less-noble phase is one of the key parameters in order to determine the severity of corrosion[5−6].

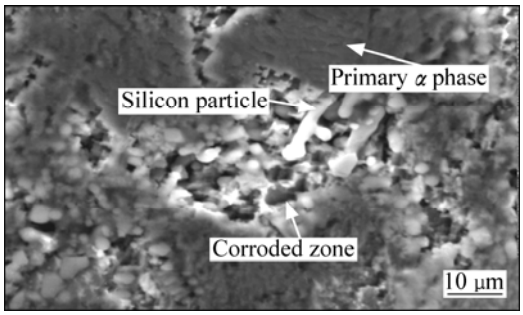

Fig.3 SEM image of corroded surfaces of thixoformed A356 samples formed at 610 °C after LSV test in 3.5% NaCl solution

In the case of thixoformed samples, area equivalent diameter of silicon particles (as cathode) is less than that of rheocast and gravity-cast A356 samples. Therefore, the enhanced corrosion resistance of thixoformed samples is believed to be associated with the reduced area ratio of eutectic silicon particles to eutectic aluminum phase around eutectic silicon particles compared with rheocast and gravity-cast A356 samples. Since corrosion has been occurred between eutectic silicon particles and eutectic aluminum phase, ratio of silicon particles area (as cathode area, A_c) to eutectic aluminum phase area around eutectic silicon particles (as anode area, A_a) is important. These values are reported in Table 4.

Table 4 Ratio of cathode area to anode area (A_c/A_a) in thixoformed, rheocast and gravity-cast A356 samples

Sample	A_c/A_a
Gravity-cast	3.67±0.73
Rheocast	3.10±0.31
Thixoformed at 600 °C	0.89±0.54
Thixoformed at 610 °C	1.77±0.39

Different processing routes cause different area equivalent diameter of silicon particles and consequently different A_c/A_a ratios. Table 5 shows the PFSR in thixoformed, rheocast and gravity-cast A356 samples in different A_c/A_a ratios. As it is seen, in low A_c/A_a ratios the PFSR is high. Therefore, an increase or decrease of the areas occupied by these phases leads to a decrease or

increase in corrosion current density, respectively. In order to identify galvanic corrosion current density between local cathode and anode in the specimens, particles of silicon and particles of aluminum are coupled with each other in a corrosion cell and values of current as a function of time were registered. For each sample, these particles considered in such a manner that the ratio between them is equal to values shown in Table 4.

Table 5 PFSR in thixoformed, rheocast and gravity-cast A356 samples in different A_c/A_a ratios

A_c/A_a	$(\varphi_p-\varphi_{ocp})$/mV
0.89	288
1.77	195
3.10	68
3.67	49

By this simulation, galvanic corrosion current, I, and consequently, local galvanic corrosion current density, J_c, between silicon particles and eutectic aluminum phase around silicon particles can be calculated. The results of this simulation and galvanic corrosion current between silicon particles and eutectic aluminum phase are shown in Table 6. Compared with the thixoformed samples, the increase in galvanic corrosion current (Fig.4) and galvanic corrosion current density in the rheocast and gravity-cast samples is related to the higher area equivalent diameter of silicon particles or A_c/A_a ratio.

Table 6 Local galvanic corrosion current density between silicon particles and eutectic aluminum phase in gravity-cast, rheocast and thixofromed A356 alloy with different A_c/A_a ratio

A_c/A_a	Corrosion current/μA
0.97	17.85
1.58	26.23
2.90	56.96
3.97	65.19

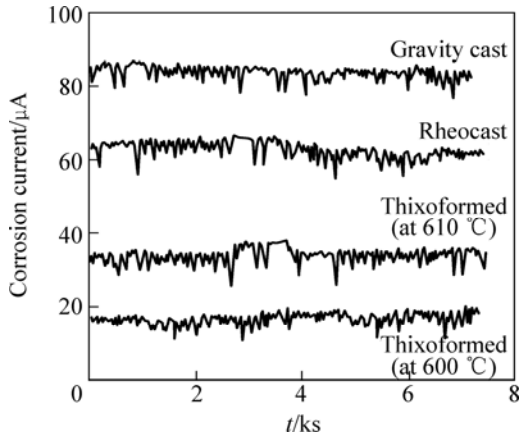

Fig.4 Corrosion current between galvanic couples of silicon and aluminum as function of time in 3.5% NaCl solution

The coarsened silicon particles make difficult the growth of the protective oxide layer in aqueous solutions and act as weak points in the passive film[15]. Weak points in the passive film are the origin of localized corrosion, as at these points the corrosion proceeds with a higher rate than elsewhere[15−16]. In the case of thixoformed samples formed at 610 °C as well as rheocast and gravity-cast samples, the area equivalent diameter of silicon particles is higher than that of the thixoformed samples formed at 600 °C. Therefore, the possibility of formation of a firmly passive film is decreased.

In the case of rheocast and gravity-cast samples, another parameter must be considered. Pitting occurs preferentially in pre-existing casting defects[9, 17]. As it is seen in Table 2, porosity in the rheocast and gravity-cast samples is higher than that in the thixoformed samples. The collective effects of higher porosity level as well as higher A_c/A_a ratio of silicon particles in rheocast and gravity-cast samples, compared with the thixoformed samples, are responsible for the reduction of PFSR and φ_P.

4 Conclusions

In this study, the pitting behavior of the thixoformed A356 alloy was studied and compared with of the rheocast and gravity-cast samples with the same composition.

By thixoforming process, the resistance to pitting corrosion is largely improved due to the reduced area ratio of noble silicon particles to less-noble eutectic aluminum phase around silicon particles. Moreover, local galvanic corrosion current density between local galvanic couples decreases due to the reduction of A_c/A_a ratio. Compared with the thixoformed samples, high levels of porosity as well as higher A_c/A_a ratio in the gravity-cast and rheocast samples are responsible for the reduction of PFSR and φ_P. In the case of gravity-cast and rheocast samples, silicon particles with high area equivalent diameter act as weak points in passive film, implying the higher rate of pitting corrosion.

References

[1] YANG Z, SEO P K, KANG C G. Grain size control of semi-solid A356 alloy manufactured by electromagnetic stirring [J]. Materials Science and Technology, 2005, 21: 219−225.

[2] PARK C, KIM S, KOWN Y, LEE Y, LEE J. Fracture behavior of thixoformed 357-T5 Al alloys [J]. Metallurgical and Materials Transaction A, 2004, 35: 1017−1027.

[3] TAHAMTAN S, GOLOZAR M A, KARIMZADEH F, NIROUMAND B. Microstructure and tensile properties of

thixoformed A356 alloy [J]. Materials Characterization, 2008, 59: 223−228.

[4] KAPRANOS P, KIRKWOOD D H, ATKINSON H V, RHEINLANDER J T, BENTZEN J J, TOFT P T. Thixoforming of an automotive part in A390 hypereutectic Al-Si alloy [J]. Materials Processing and Technology, 2003, 135: 271−277.

[5] YU Y, KIM S, LEE Y, LEE J. Phenomenological observation on mechanical and corrosion properties of thixoformed 357 alloys: A comparison with permanent mold cast 357 alloys [J]. Metallurgical and Materials Transactions A, 2002, 33: 1399−1412.

[6] PARK C, KIM S, KWON Y, LEE Y, LEE J. Mechanical and corrosion properties of rheocast and low-pressure cast A356-T6 alloy [J]. Materials Science and Engineering A, 2005, 391: 86.

[7] PARK C, KIM S S, LEE Y S. [C]//Proc 7th Int Conf on Semisolid Processing of Alloys and Composites. Tsukuba, Japan, 2004: 298−301.

[8] WINKLER S L, RYAN M P, FLOWER H M. Pitting corrosion in cast 7××× aluminum alloys and fiber reinforced MMCs [J]. Corrosion Science, 2004, 46: 893−902.

[9] PYUN S I, LEE W J. The effect of prior Cl^- ion incorporation into native oxide film on pure aluminium in neutral chloride solution on pit initiation [J]. Corrosion Science, 2001, 43: 353−363.

[10] McCAFFERTY E. Sequence of steps in the pitting of aluminum by chloride ions [J]. Corrosion Science, 2003, 45: 1421−1438.

[11] TZANEVA B R, FACHIKOV L B, RAICHEFF R G. Effect of halide anions and temperature on initiation of pitting in Cr-Mn-N and Cr-Ni steels [J]. Corrosion Engineering Science and Technology, 2006, 41: 62−66.

[12] BURSTEIN G T, LIU C, SOUTO R M, VINES S P. Origins of pitting corrosion [J]. Corrosion Engineering Science and Technology, 2004, 39: 25−30.

[13] YURT A, BEREKET G, OGRETIR C. Quantum chemical studies on inhibition effect of amino acids and hydroxy carboxylic acids on pitting corrosion of aluminum alloy 7075 in NaCl solution [J]. Molcular Structure, 2005, 25: 215−221.

[14] SANKARAN K K, PEREZ R, JATA K V. Effects of pitting corrosion on the fatigue behavior of aluminum alloy 7075-T6: Modeling and experimental studies [J]. Materials Science and Engineering A, 2001, 297: 223−229.

[15] BARBUCCI A, BRUZZONE G, DELUCCHI M, PANIZZA M, CERISOLA G. Breakdown of passivity of aluminium alloys by intermetallic phases in neutral chloride solution [J]. Intermetallics, 2000, 8: 305−312.

[16] SHAO M, FU Y, HU R, LIN C. A study on pitting corrosion of aluminum alloy 2024-T3 by scanning microreference electrode technique [J]. Materials Science and Engineering A, 2003, 344: 323−327.

[17] PARDO A, MERINO M C, MERINO S, VIEJO F. Influence of reinforcement proportion and matrix composition on pitting corrosion behavior of cast aluminum matrix composites (A3xx.x/SiC_p) [J]. Corrosion Science, 2005, 47: 1750−1764.

(Edited by YANG Bing)